Absorption-sensitive diffuse reflection imaging of concealed powders using a terahertz quantum cascade laser

Paul Dean,[1*] Muhammad U. Shaukat,[1] Suraj P. Khanna,[1] Subhasish Chakraborty,[2] Mohammad Lachab,[1] Andrew Burnett,[1] Giles Davies[1] and Edmund H. Linfield[1]

[1]*School of Electronic and Electrical Engineering, University of Leeds, Leeds, LS2 9JT, UK*
[2]*School of Electrical and Electronic Engineering, University of Manchester, Manchester, M60 1QD, UK*
[*]*Corresponding author: p.dean@leeds.ac.uk*

Abstract: We report diffuse reflection imaging in air of concealed powdered samples using a terahertz quantum cascade laser. The sensitivity of the detection scheme to sub-surface absorption within samples is confirmed using fully-characterized powdered admixtures of polystyrene and polymethyl methacrylate (PMMA). Measurements of the backscattering intensity from these samples are then used in conjunction with Kubelka-Munk scattering theory, as well as several models based on the quasi-crystalline approximation, to extract the absorption coefficient of PMMA. Our research demonstrates the feasibility of high-resolution frequency-domain terahertz imaging for the detection and identification of concealed powders in a reflection geometry.

OCIS codes: (110.6795) Terahertz imaging; (140.5965) Semiconductor lasers, quantum cascade (280.1350) Backscattering; (300.1030) Absorption

References and links

1. B. B. Hu and M. C. Nuss, "Imaging with THz waves," Opt. Lett. **20**, 1716-1718 (1995).
2. D. Mittleman, *Sensing with THz Radiation* (Springer, Berlin, 2003).
3. K. Kawase, Y. Ogawa, Y. Watanabe, and H. Inoue, "Non-destructive terahertz imaging of illicit drugs using spectral fingerprints," Opt. Express **11**, 2549-2554 (2003), http://www.opticsinfobase.org/abstract.cfm?URI=oe-11-20-2549.
4. Y. C. Shen, T. Lo, P. F. Taday, B. E. Cole, R. Tribe, and M. C. Kemp, "Detection and identification of explosives using THz pulsed spectroscopic imaging," Appl. Phys. Lett. **86**, 241116-241118 (2005).
5. D. J. Cook, B. K. Decker, G. Dadusc, and M. G. Allen, "Through container THz sensing: applications for bio detection," in *Int. Soc. Opt. Eng.* Proc. SPIE **5268**, 36-42 (2004).
6. V. P. Wallace, R. M. Woodward, A. J. Fitzgerald, E. Pickwell, R. J. Pye, and D. D. Arnone, "Terahertz pulsed imaging of basal cell carcinoma ex vivo and in vivo," Br. J. Dermatol. **151**, 424-432 (2004).
7. S. M. Kim, F. Hatami, J. S. Harris, A. W. Kurian, J. Ford, D. King, G. Scalari, M. Giovannini, N. Hoyler, J. Faist, and G. Harris, "Biomedical terahertz imaging with a quantum cascade laser," Appl. Phys. Lett. **88**, 153903-153905 (2006).
8. E. Pickwell, B. E. Cole, A. J. Fitzgerald, and V. P. Wallace, "Simulation of terahertz pulse propagation in biological systems," Appl. Phys. Lett. **84**, 2190-2192 (2004).
9. J. Chen, Y. Chen, H. Zhao, G. J. Bastiaans, and X.-C. Zhang, "Absorption coefficients of selected explosives and related compounds in the range of 0.1-2.8 THz," Opt. Express **15**, 12060-12067 (2007), http://www.opticsinfobase.org/abstract.cfm?URI=oe-15-19-12060.
10. A. Burnett, W. Fan, P. Upadhya, J. Cunningham, E. H. Linfield, A. G. Davies, H. Edwards, T. Munshi, and A. O'Neil, "Analysis of drugs of abuse and explosives using terahertz time-domain and Raman spectroscopy," *Int. Soc. Opt. Eng. Proc.* SPIE **6549**, 61200 (2007).
11. A. J. Fitzgerald, E. Berry, N. N. Zinovev, G. C. Walker, M. A. Smith, and J. M. Chamberlain, "An introduction to medical imaging with coherent terahertz frequency radiation," Phys. Med. Biol. **47**, R67-84 (2002).
12. T. Kleine-Ostmann, P. Knobloch, M. Koch, S. Hoffman, M. Breede, M. Hofmann, G. Hein, K. Pierz, M. Sperling, and K. Donhuijsen, "Continuous-wave THz imaging," Electron. Lett. **37**, 1461-1463 (2001).
13. A. Dobroiu, M. Yamashita, Y. N. Oshima, Y. Morita, C. Otani, and K. Kawase, "Terahertz imaging system based on a backward-wave oscillator," Appl. Opt. **43**, 5637-5646 (2004).

#92353 - $15.00 USD Received 1 Feb 2008; revised 5 Mar 2008; accepted 5 Mar 2008; published 14 Apr 2008

14. Y. Watanabe, K. Kawase, T. Ikari, H. Ito, Y. Ishikawa, and H. Minamide, "Component spatial pattern analysis of chemicals using terahertz spectroscopic imaging," Appl. Phys. Lett. **83**, 800-802 (2003).
15. B. Williams, S. Kumar, Q. Hu, and J. L. Reno, "High-power quantum cascade lasers," Electron. Lett. **42**, 89-90 (2006).
16. A. W. M. Lee, Q. Qin, S. Kumar, B. S. Williams, Q. Hu, and J. L. Reno, "Real-time terahertz imaging over a standoff distance (>25 meters)," Appl. Phys. Lett. **89**, 141125-141127 (2006).
17. A. W. M. Lee and Q. Hu, "Real-time, continuous-wave terahertz imaging by use of a microbolometer focal-plane array," Opt. Lett. **30**, 2563-2565 (2005).
18. M. A. Belkin, J. A. Fan, S. Hormoz, F. Capasso, S. P. Khanna, M. Lachab, A. G. Davies, and E. H. Linfield, "Terahertz quantum cascade lasers with copper metal-metal waveguides operating up to 178 K," Opt. Express **16**, 3242-3248 (2008), http://www.opticsinfobase.org/abstract.cfm?URI=oe-16-5-3242.
19. H-B. Liu, Y. Chen, G. J. Bastiaans, and X.-C. Zhang, "Detection and identification of explosive RDX by THz diffuse reflection spectroscopy," Opt. Express **14**, 415-423 (2006), http://www.opticsinfobase.org/abstract.cfm?URI=oe-14-1-415.
20. J. Pearce and D. M. Mittleman, "Propagation of single-cycle terahertz pulses in random media," Opt. Lett. **26**, 2002-2004 (2001).
21. J. Pearce, Z. Jian, and D. M. Mittleman, "Statistics of multiply scattered broadband terahertz pulses," Phys. Rev. Lett. **91**, 043903-1-4 (2003).
22. S. Barbieri, J. Alton, H. E. Beere, J. Fowler, E. H. Linfield, and D. A. Ritchie, "2.9 THz quantum cascade laser operating at 70 K in continuous wave," Appl. Phys. Lett. **85**, 1674-1676 (2004).
23. M. Naftaly, A. Malcoci, and H. Eisele, "A sensitive broadband detector for room-temperature operation of a simple terahertz Fourier-transform spectrometer," The Joint 31st International Conference on Infrared and Millimeter Waves and 14th International Conference on Terahertz Electronics, p.35 (2006).
24. K. L. Nguyen, M. L. Johns, L. F. Gladden, C. H. Worrall, P. Alexander, H. E. Beere, M. Pepper, D. A. Ritchie, J. Alton, S. Barbieri, and E. H. Linfield, "Three-dimensional imaging with a terahertz quantum cascade laser," Opt. Express **14**, 2123-2129 (2006), http://www.opticsinfobase.org/abstract.cfm?URI=oe-14-6-2123.
25. S. Barbieri, J. Alton, C. Baker, T. Lo, H. E. Beere, and D. Ritchie, "Imaging with THz quantum cascade lasers using a Schottky diode mixer," Opt. Express **13**, 6497-6503 (2005), http://www.opticsinfobase.org/abstract.cfm?URI=oe-13-17-6497.
26. J. Coltman, "The specification of imaging properties by response to a sine wave input," J. Opt. Soc. Am. **46**, 468-72 (1954).
27. J. R. Birch, "The far-infrared optical constants of polypropylene, PTFE and polystyrene," Infrared Phys. **33**, 33-38 (1992).
28. L. Tsang, J. A. Kong, and R. T. Shin, *Theory of Microwave Remote Sensing* (New York, Wiley, 1985)
29. G. Kortum, *Reflectance Spectroscopy* (Springer, Berlin, 1969).
30. P. Kubelka and F. Munk, "Ein beitrag zur optic der fabanstriche," Z. Tech. Physik **12**, 593-601 (1931).
31. J. D. Lindberg, R. E. Douglass, and D. M. Garvey, "Absorption-coefficient-determination method for particulate materials," Appl. Opt. **33**, 4314-4319 (1994).
32. J. D. Lindberg, "Absolute diffuse reflectance from relative reflectance measurements," Appl. Opt. **26**, 2900-2905 (1987).
33. L. L. Foldy, "The multiple scattering of waves. I. General theory of isotropic scattering by randomly distributed scatterers" Phys. Rev. **67**, 107-119 (1945).
34. M. Lax, "Multiple scattering of waves. II. The effective field in dense systems," Phys. Rev. **85**, 621-629 (1952).
35. M. S. Wertheim, "Exact solution of the Percus-Yevick integral equation for hard spheres," Phys. Rev. Lett. 1**0**, 321-323 (1963).
36. L. Tsang and J. A. Kong, "Scattering of electromagnetic waves from a half space of densely distributed dielectric scatterers," Radio Science **18**, 1260-1272 (1963).
37. P. R. Siqueira and K. Sarabandi, "Method of moments evaluation of the two-dimensional quasi-crystalline approximation," IEEE Trans. Antenn. Prop. **44**, 1067-1077 (1996).

1. Introduction

Over recent years there has been a great deal of interest in terahertz (THz) imaging applications, particularly in the fields of non-destructive inspection, security screening and biomedicine [1-8]. The suitability of THz radiation to such applications stems primarily from the transparency of many non-polar materials at THz frequencies. THz radiation is also sensitive to absorption arising from molecularly-specific vibrational modes in a wide range of organic and inorganic chemicals including explosives and drugs-of-abuse [9,10]. THz

#92353 - $15.00 USD Received 1 Feb 2008; revised 5 Mar 2008; accepted 5 Mar 2008; published 14 Apr 2008

imaging is therefore particularly well-suited to chemical fingerprinting and sensing applications.

A range of THz imaging systems have been previously reported [1-8]. Many of these employ broadband photoconductive sources alongside time-domain detection, enabling frequency-dependent imaging over a broad spectrum [11]. However, systems of this type suffer from low THz powers (~10-100 μW) as well as the reliance on an expensive ultra-fast near-infrared/visible laser source. Incoherent imaging using a narrowband tuneable source has also been demonstrated [12-13] and applied to component spatial pattern analysis of chemical mixtures [3,14]. Whilst such systems offer potential for chemical sensing applications, in addition to the practical advantage of not requiring optical gating of the detector, performance is again limited by only moderate THz powers and the limited availability of widely-tuneable sources. Conversely, terahertz quantum cascade lasers (QCLs) deliver high output powers, which can exceed 100 mW in continuous-wave operation [15]. Stand-off imaging over a distance of 25 m has been previously reported using such sources [16], as has real-time imaging through use of a micro-bolometer array [17]. To date, emission frequencies range from 1.2 to 5.0 THz and operating temperatures as high as 178 K have been achieved [18]. Their narrowband emission and tunability also indicate that these sources offer great potential for the development of fast spectroscopic stand-off imaging systems with high sensitivity and chemical specificity.

Owing to the relative practical simplicity, the majority of THz imaging systems reported to date employ a transmission geometry. However, this geometry is only applicable when the sample under investigation is suitably thin and exhibits low absorption at THz frequencies. In order to perform imaging of bulky or highly-absorbing samples, one is restricted to a reflective geometry in which radiation reflected or back-scattered from the sample is detected. For stand-off imaging, however, the exact alignment required for collection of specular reflections cannot be guaranteed in practice. A practical stand-off imaging system should therefore monitor diffuse radiation returning from the sample. Diffuse imaging also enables the detection of samples contained within packaging that would adversely affect measurements in a specular geometry, as well as samples from which there is a strong component of sub-surface scattered radiation such as powders. Sensitivity to such radiation is essential for spectroscopic identification of materials when a narrowband source and incoherent detection are employed. A diffuse sensing scheme is thus highly applicable for drug- and explosive-fingerprinting applications using THz QCLs.

In this paper we report diffuse reflection imaging in air using a QCL at 2.8 THz. The detection of concealed powdered samples is demonstrated, including the detection of powders concealed within a container from which there is a strong specular reflection. The sensitivity of the detection scheme to sub-surface absorption of radiation is confirmed using fully characterized admixtures of polystyrene and polymethyl methacrylate (PMMA) powders. These measurements are then used to assess the suitability of Kubelka-Munk theory, and a number of back-scattering theories based on the quasi-crystalline approximation (QCA), to describe diffuse reflection from absorbing samples at THz frequencies. In particular, these theories are used to extract the absorption coefficient of PMMA and these predictions are compared with measurements obtained using THz time-domain spectroscopy (TDS). To the best of our knowledge, this work represents the first demonstration of absorption-sensitive reflection imaging using a THz QCL. Our investigation also demonstrates the applicability of frequency-domain THz imaging to the detection and identification of concealed powdered materials such as drugs and explosives.

2. Background

The interaction between radiation and bulk powdered samples can be described in terms of three mechanisms: directional specular reflection from powder surfaces, non-directional 'diffuse Fresnel reflection' from rough sample surfaces [19], and sub-surface scattering and absorption of radiation by the powdered medium. The relative strengths of these mechanisms depend on the degree of surface roughness, the complex refractive index of the material, as

#92353 - $15.00 USD Received 1 Feb 2008; revised 5 Mar 2008; accepted 5 Mar 2008; published 14 Apr 2008

well as the mean particle size of the powder. For smooth samples (root-mean-square surface roughness much smaller than the radiation wavelength λ), the specular reflection at the air-powder interface is strongly directional and can be discriminated against with the use of off-axis collection optics. For larger particle sizes, this reflection becomes increasingly non-directional owing to reflections from small randomly orientated mirror-like micro-facets on the sample surface. For both rough and smooth surfaces, a portion of the incident radiation penetrates beneath the surface of the sample where it experiences both scattering and absorption by the particles of the medium. Scattering is strongest when the particle size is comparable to the radiation wavelength whereas the degree of absorption is dictated by the wavelength-dependent complex refractive index of the material. Terahertz propagation in the presence of multiple scattering has been investigated elsewhere [20,21].

For chemical fingerprinting applications, the measurement scheme should be sensitive to the absorption coefficient of the material under analysis. When a coherent detection scheme is used, the imaginary part of the refractive index can be deduced from the diffuse Fresnel reflections through use of the measured or inferred phase delays [19]. When incoherent detection is used, only the amplitude of the diffuse Fresnel reflection is measured and this is only weakly dependent on the imaginary part of the refractive index for most materials. For chemical fingerprinting applications, incoherent diffuse measurements must therefore make use of sub-surface scattered radiation, the amplitude of which is strongly influenced by absorption within the sample.

3. Terahertz imaging system

3.1 Experimental setup

Figure 1 shows a schematic diagram of the imaging apparatus used for this work. The laser was a 2.5-mm-long bound-to-continuum QCL emitting at 2.8 THz [22], which was cooled to ~5 K in a closed-cycle pulse tube refrigerator. Radiation from the QCL was collimated with an f/1.7 parabolic reflector and focused onto the sample at a 30° angle of incidence using an f/4.3 reflector. The focal length of this reflector provided a working distance of 33 cm. A second f/4.3 parabolic was used to collect specular reflections from the sample surface, which were coupled onto a room temperature Murata pyroelectric sensor [23] (D1). Diffusely scattered and non-directional reflected radiation was collected using a 90° f/2 parabolic reflector and coupled into a helium-cooled silicon bolometer (D2). The off-axis configuration of this reflector ensured that no direct specular reflection was collected. Our system thus permits simultaneous detection of both scattered and specularly reflected THz radiation. Whilst a cryogenically-cooled detector was used in this system, we note that a usable detection sensitivity could be achieved using a room-temperature Golay cell [24] or Schottky diode mixer [25].

Current pulses were supplied to the QCL at a frequency of 50 kHz and a duty cycle of 40%. These pulses were electronically modulated at a frequency of 160 Hz with lock-in detection being employed to improve the detection sensitivity. This lock-in modulation frequency was selected to allow simultaneous lock-in detection from both detectors. Measurements indicate that the signal-to-noise ratio of the pyroelectric sensor is optimised at ~20 Hz whereas that of the bolometer is optimised at ~200 Hz. Both detectors are therefore operated in a non-optimised regime. Under normal operation both detectors were susceptible to noise induced by the high-frequency current pulses driving the QCL. This noise source was reduced, with only a small sacrifice in output power, by use of a 5-pole low-pass filter with a 1 MHz 3-dB point on the output of the current source. Under the conditions described. the peak power incident on the sample is estimated to be ~1 mW. For image acquisition, the sample was mounted on a two-axis translation stage that was raster scanned with a 250-μm step-size. No purging of the system was used.

#92353 - $15.00 USD Received 1 Feb 2008; revised 5 Mar 2008; accepted 5 Mar 2008; published 14 Apr 2008

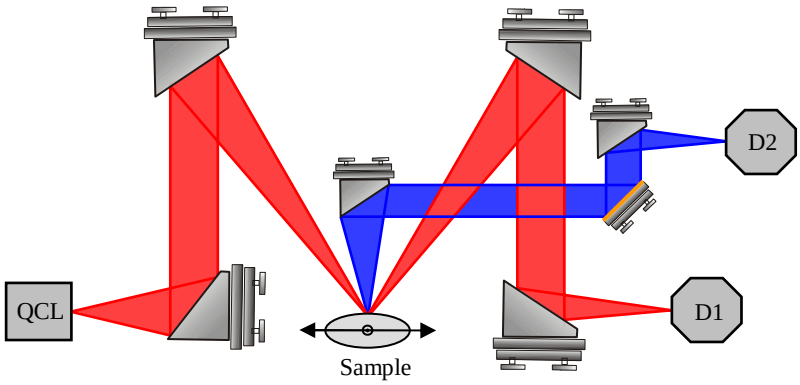

Fig. 1. Experimental apparatus for simultaneous specular (red) and diffuse (blue) imaging using a THz-frequency quantum cascade laser (QCL). D1 – room-temperature pyroelectric sensor; D2 – helium-cooled silicon bolometer.

3.2 System resolution

The spatial resolution of the system was analysed using a series of gold-on-glass resolution targets. With the resolution target positioned in the object plane of the system, line profiles were recorded for both horizontal and vertical orientations using a 10-μm step-size. For each line scan the square-wave modulation depth was measured and the Coltman expansion [26] applied to deduce the sinusoidal modulation depth. The modulation transfer function (MTF) was then obtained by normalising to the modulation for an infinite-period sinusoidal target. Figure 2 shows the horizontal and vertical MTFs measured for our system. Defining the resolution limit at the 20% modulation threshold indicates spatial resolutions equal to 350 μm and 305 μm along horizontal and vertical directions, respectively. These values are consistent with a circularly symmetric beam projected onto the sample plane at an incidence angle of 30°.

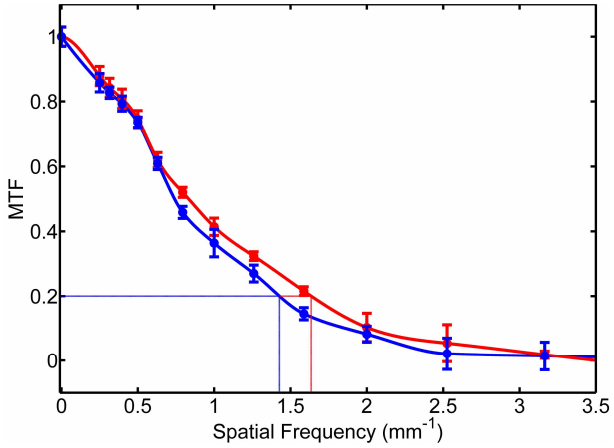

Fig. 2. Measurement of the modulation transfer function (MTF) of the imaging setup using vertically (blue) and horizontally (red) oriented targets. The lines are intended only to guide the eye. The 20% modulation threshold indicates spatial resolutions equal to 350 μm and 305 μm respectively.

#92353 - $15.00 USD Received 1 Feb 2008; revised 5 Mar 2008; accepted 5 Mar 2008; published 14 Apr 2008

4. Results

4.1 Diffuse imaging of concealed powders

The detection of powdered samples using a diffuse imaging scheme was initially demonstrated using 800 mg of loose polyethylene powder contained within a 35 mm x 50 mm re-sealable polythene bag. Figure 3 shows a THz image of this sample concealed behind a fibrous HDPE FedEx® envelope and taken with a 250-μm step-size. As can be seen, the powder is clearly imaged and the obscuring layer has little effect other than a weak contribution arising from reflections off its surface. The regions of high intensity are specular highlights arising from creases in the front surface of the polythene bag.

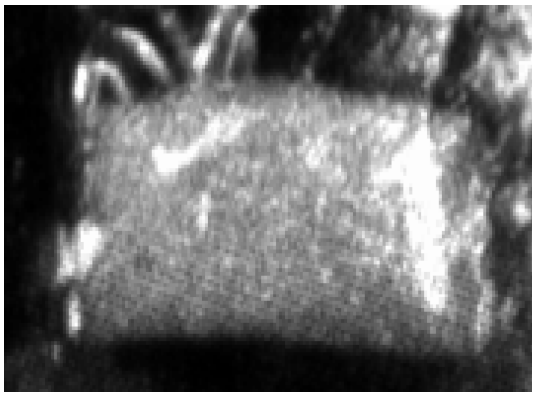

Fig. 3. Diffuse image of polyethylene powder enclosed inside a polythene bag and concealed behind a HDPE FedEx® envelope, taken with a 250-μm pixel size.

The image acquisition time for this 180 x 108 pixel image was 27 minutes (~12 pixels per second (pps)), which is limited by the ~75 ms traveling time for the translation stage used in this measurement. For comparison, the signal averaging time and computer processing time amounted to ~6 ms per pixel. The peak THz power coupled into the detector after scattering from this low-absorbing sample was estimated to be ~1 μW. This provides a measurement dynamic range of 20 dB at this maximum imaging rate. We note that greater dynamic ranges can be achieved at the expense of imaging speed with longer time-averaging of each pixel. For example, at 5 pps the dynamic range was measured to be 30 dB.

4.2 Absorption-sensitive imaging of powders

The sensitivity of our system to absorption within powdered samples was demonstrated using polystyrene and PMMA as model compounds. Polystyrene is known to exhibit low absorption at THz frequencies [27] whereas PMMA is strongly absorbing. Powders were selected that had well-characterised and closely matched particle sizes; the polystyrene and PMMA had manufacturer-specified particle sizes of 6.06 ± 0.08 μm and 5.4 ± 0.5 μm, respectively. Nine sample admixtures were prepared with mass fractions ranging from 0 to 1 in equal steps of 0.125. These were then loosely packed inside a sample holder comprising a polystyrene box divided into separate compartments, each measuring approximately 10 mm x 10 mm x 10 mm, with a removable polystyrene lid (see Fig. 4(a)); the dimensions of each powder sample measured approximately 9 mm x 9 mm x 9 mm. Measurements of the volume filling fraction indicate a value of 0.4 for these uncompressed powders.

Figure 4(b) shows the specular image of this sample taken with a 250-μm pixel size. As can be seen, the image is dominated by strong reflections off the surface of the lid and the powders cannot be resolved. The corresponding diffuse image is shown in Fig. 4(c). In this case, there is a negligible contribution from specular reflections and the powders are clearly imaged. In addition, there is a strong correlation between the image intensity and the fraction

#92353 - $15.00 USD Received 1 Feb 2008; revised 5 Mar 2008; accepted 5 Mar 2008; published 14 Apr 2008

of strongly absorbing material. This correlation is investigated in more detail in Sec. 5. The peak powers measured at the detectors D_1 and D_2 were ~15 μW and ~400 nW, respectively, in the case of the lowest absorbing samples.

The image intensity for each powder admixture was measured by sampling over a 5 mm x 5 mm (20 x 20 pixels) region in the centre of each compartment in order to reduce the effects of laser speckle and structural variation. Five independent sets of measurements were performed and averaged to yield the reflectivity for each sample, measured relative to a PTFE powder reference. Measurements performed on pressed pellets using TDS [10] reveal that the refractive index of the two materials is almost identical at 2.8 THz; 1.42 ± 0.02 for polystyrene and 1.38 ± 0.02 in the case of PMMA. By virtue of this and the closely matched particle sizes, the scattering mean-free-path and angular distribution within these nine samples are expected to be almost identical. Furthermore, the small particle sizes used here ensure a small contribution to the collected radiation from diffuse surface reflections. The observed differences in the measured image intensities for the nine mixture compositions can therefore be solely attributed to different degrees of absorption within these samples.

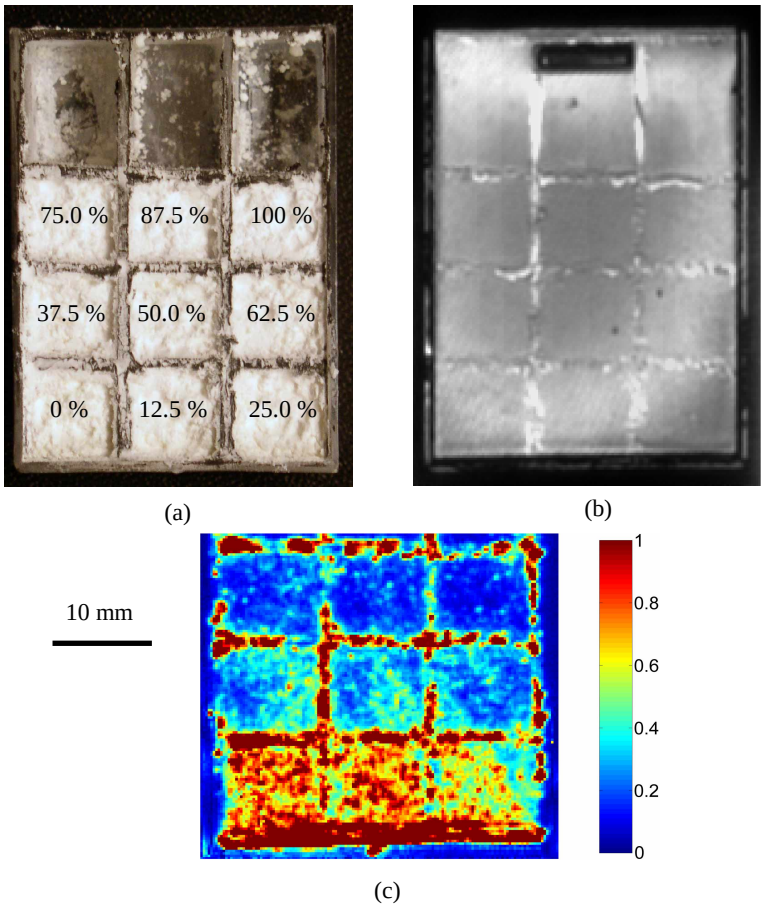

Fig. 4. (a) Photograph of the sample holder (lid removed) loaded with powder admixtures. The % mass of PMMA is shown for each admixture. (b) Specular THz image of the sample shown in (a). (c) Diffuse THz image of the sample shown in (a). The non-uniform intensity distributions observed here are attributed to the presence of diffuse surface reflections and scattering from micro-cavities formed within the samples. Such effects are averaged-out with repeated measurements. All three images are displayed on the same scale. The THz images have a pixel size of 250 μm.

#92353 - $15.00 USD Received 1 Feb 2008; revised 5 Mar 2008; accepted 5 Mar 2008; published 14 Apr 2008

5. Analysis

5.1 Kubelka-Munk theory

A number of theoretical models have been developed for describing the backscattering of radiation from a dense medium of randomly distributed dielectric particles [28,29]. The most commonly applied of these is Kubelka-Munk (KM) theory owing to the simplicity of its formulism [30]. This model is derived from the radiative transport equation and describes the propagation of a uniform, diffuse irradiance through a one-dimensional semi-infinite isotropic slab.

KM theory relates the diffuse reflectivity R_∞ of an infinitely thick absorbing sample to the KM absorption coefficient K and scattering coefficient S according to the remission function

$$F(R_\infty) = \frac{(1-R_\infty)^2}{2R_\infty} = \frac{K}{S}. \quad (1)$$

For the admixtures measured in this investigation, the scattering coefficient S is independent of the mixture composition owing to the matched particle size and matched real refractive indices of the two powders. Therefore, for the present case, Eq. (1) can be written as [29]:

$$F(R_\infty) \approx \frac{3}{2n^2 S}\left[c\alpha_1 + (1-c)\alpha_2\right]. \quad (2)$$

Here K has been expressed in terms of the volume fraction c of species 1 (PMMA), relative to the total volume fraction of powder, and the Lambert's law absorption coefficients α_1 and α_2 of both materials using the approximation $K \approx 3\alpha/2n^2$, where n is the real refractive index [31].

The remission function $F(R_\infty)$ is extremely sensitive to changes in reflectivity for small values of R_∞. Care must therefore be taken to ensure correct calculation of R_∞ from the measurement data. In theory, the reference sample should be completely diffusing and non-absorbing - conditions unachievable in practice. However, in the present case we can make use of the fact that, according to Eq. (2) and assuming $\alpha_1 >> \alpha_2$, $d\left[\ln\left(F(\gamma R)\right)\right]/d\left[\ln(c)\right] \approx 1$ [29,32]. Here, R_∞ has been written in terms of a constant γ to be determined, and the reflectivity R measured relative to a PTFE reference. By fitting this relationship to the experimental data, the value of γ can be estimated. The resulting values for R_∞, calculated from the measured values of R and the fitted value of γ using the relation $R_\infty = \gamma R$, are shown in Fig. 5 as a function of the volume fraction of PMMA.

Also shown in Fig. 5 are the corresponding values of the remission function $F(R_\infty)$. As expected, we observe a clear linear relationship between $F(R_\infty)$ and the volume fraction of PMMA. Figure 5 also shows a fit of this data to Eq. (2), for which a value $\alpha_2 = 4$ cm^{-1} has been used, as measured using THz TDS. The intercept of the fitted line predicts a value $S = 5 \pm 1$ cm^{-1} and the slope yields the estimate $\alpha_1 = 42 \pm 11$ cm^{-1} for the absorption coefficient of PMMA. The uncertainties in these values reflect the distribution of measured image intensities for each sample as well as the sensitivity of $F(R_\infty)$ to small changes in R_∞.

#92353 - $15.00 USD Received 1 Feb 2008; revised 5 Mar 2008; accepted 5 Mar 2008; published 14 Apr 2008

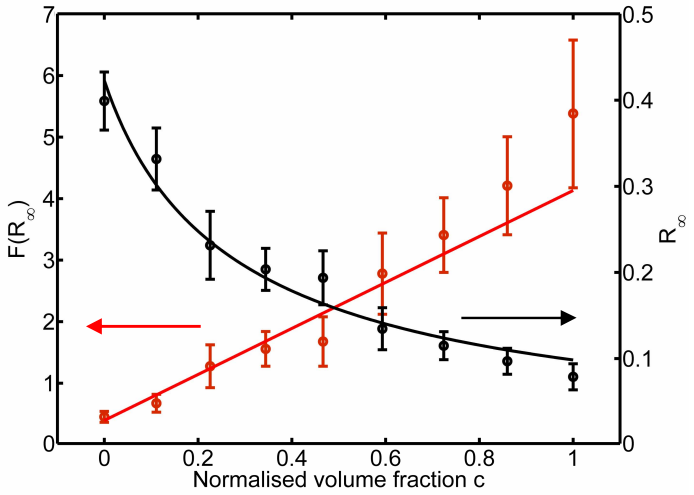

Fig. 5. Measurement of the sample reflectivity R_∞ (black, right axis) as a function of volume fraction of PMMA. The corresponding values of the Kubelka-Munk remission function $F(R_\infty)$ are also shown (red, left axis). The lines represent fits of the data to Eq. (2), in which the estimated value of γ=1.6 is used, and S=5±1 cm^{-1} and α_1= 42±11 cm^{-1}are treated as free parameters.

5.2 Quasi-crystalline approximation

More rigorous scattering models that include the effects of phase coherence have been based on wave theory and the multiple scattering equations [28]. One of the simplest of these models describes multiple scattering from isotropic point scatterers and neglects any correlation between particle positions. This is known as the effective field approximation (EFA) [33] and is most applicable to low concentrations of scatterers. A higher order approximation to the EFA that does account for correlated particle positions is the quasi-crystalline approximation (QCA) [34]. For a sparse concentration of scatterers it is reasonable to assume that the particle positions are independent of each other. Hence, in this limit the QCA reduces to the EFA. For larger concentrations, the QCA can be used in conjunction with realistic pair distribution functions such as the Percus-Yevick (PY) distribution for spherical particles [35]. A further correction to the QCA-PY model is the coherent potential (QCA-CP) formulism [28], which more accurately accounts for the effective electrical permittivity that a wave experiences in a dense medium of particles.

A closed-form expression for the backscattering cross-section σ of electromagnetic waves scattered from a half space of densely distributed dielectric scatterers under the QCA has been previously reported [28,36]. Derivation of this expression assumes a polarized plane wave obliquely incident on the scattering medium, and is valid only in the low-frequency limit ($\lambda >>$ particle size) and under the distorted Born approximation. In our case we use an incident angle of 30° and take the backscattered power to be proportional to σ for this geometry. The absorption coefficient of polystyrene is again taken to be 4 cm^{-1}.

Figure 6 show fits of the measured image intensities, cast in terms of the backscattering cross-section, as a function of volume fraction of PMMA under the EFA, QCA-PY and QCA-CP. The magnitude of σ is significantly larger in the case of the EFA, which is to be expected owing to the assumption of uncorrelated particle positions. Nevertheless, it can be seen that the EFA, QCA-PY and QCA-CP all predict a similar functional dependence of σ on the volume fraction of PMMA. The values of α_1 obtained from these fits are 19.7±2.3 cm^{-1}, 18.1±2.1 cm^{-1} and 17.9±1.9 cm^{-1}, respectively. For comparison, measurements performed on pressed pellets using THz TDS predict a value α_1=41 cm^{-1} at the QCL radiation wavelength.

#92353 - $15.00 USD Received 1 Feb 2008; revised 5 Mar 2008; accepted 5 Mar 2008; published 14 Apr 2008

Hence, we note that these scattering models consistently underestimate the absorption coefficient for the experimental conditions employed here.

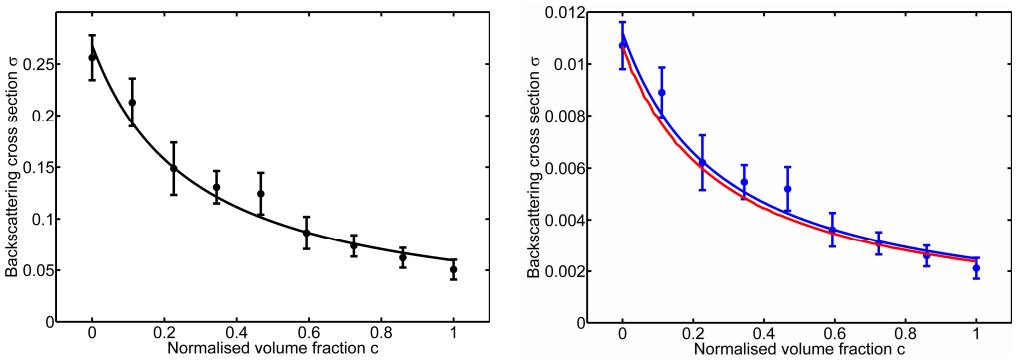

(a) (b)

Fig. 6. Measurement of the backscattering cross-section as a function of volume fraction of PMMA under the (a) EFA (black), (b) QCA-PY (blue) and QCA-CP (red; data points not shown).

6. Discussion

All four of the scattering models evaluated in this paper successfully reproduce the experimental observation that the diffuse reflectivity decreases for increasing absorption strength of the sample material. The absorption coefficient obtained from KM theory agrees well with the value measured using THz TDS. In the case of the QCA-based backscattering models, the absorption coefficient is underestimated by a factor of ~2. This difference could be attributed to the collection of additional diffuse surface reflections from the samples, which leads to underestimation of the absorption coefficient in the case of the QCA-based models, but overestimation of both K and S using the KM analysis presented here. This difference could also indicate the inadequacy of the QCA-based models at larger volume fractions, as has been reported elsewhere [37].

The consistency between the values of α_1 predicted by the three QCA-based models is a result of the small size parameter (~0.03) and small relative permittivity of the powdered samples used. Under these conditions, the implementation of the PY pair distribution function has the primary effect of uniformly reducing the backscattering cross-sections predicted. In the limit of very small particle size, the effective permittivity calculated under QCA-PY approaches that calculated under EFA. Therefore, in this limit, the two methods yield similar values of α_1. Comparing the QCA-PY and QCA-CP models, their internal consistency can be explained by the similarity between the effective relative permittivity (~1.33) used in the latter model with that of air, which is a consequence of the small permittivity of the powder materials [28].

It should be noted that measurement of the *absolute* absorption coefficient of an unknown powered material would not, in general, be possible using KM theory without prior calibration of the image intensity using either the method described above or a suitable reflection standard. For reflection measurements from a single powder, the relationship between K and S demonstrated by Eq. (1) would then permit only a qualitative assessment of the material absorption coefficient. This is also true in the case of the QCA-based models since the sample parameters such as particle size and packing density would not be known in general. Nevertheless, we note that for chemical fingerprinting applications one is concerned only with the ratio of image intensities measured from the same sample at two or more known wavelengths. The analysis presented in Sec. 5 suggests that all four of the models evaluated would enable a qualitative assessment of wavelength-dependent absorption within samples,

#92353 - $15.00 USD Received 1 Feb 2008; revised 5 Mar 2008; accepted 5 Mar 2008; published 14 Apr 2008

and thus provide fingerprint information for sensing applications. With careful selection of the imaging wavelengths, specific materials could thus be targeted. Since application of the QCA-based models do not require knowledge of the absolute sample reflectivity, perhaps these hold greater promise for the analysis of multi-wavelength diffuse reflection measurements. It should be noted, however, that the present analytical formulism of the QCA-based models is applicable only in the limit $\lambda >>$ particle size. Further diffuse measurements on samples with larger particle sizes, as well as implementation of a complete QCA-based model that does not adopt the low-frequency approximation, would be required to assess fully the performance of these models outside this limit.

7. Conclusions

In summary, we have demonstrated diffuse reflection imaging of powdered samples in air using a terahertz quantum cascade laser. For a weakly-absorbing polyethylene powder enclosed inside a plastic bag and concealed behind a HDPE FedEx® envelope, a dynamic range of ~20dB was measured at the maximum imaging rate of ~12 pps, which was limited by translation of the sample in our apparatus. The sensitivity of the detection scheme to absorption within samples was confirmed using measurements of the backscattered intensity for a range of characterized polystyrene-PMMA powdered admixtures. These measurements have been fitted to a number of scattering theories and the absorption coefficient of PMMA extracted in each case. Kubelka-Munk theory yielded a value of 42 ± 11 cm^{-1} whereas theories based on the quasi-crystalline approximation consistently underestimated this value by a factor ~2. Measurements obtained using THz TDS yield a value of 41 cm^{-1}. These results confirm that such models could enable qualitative assessment of wavelength-dependent absorption within powdered samples, sufficient to provide fingerprinting information. Our research therefore demonstrates the potential of multi-wavelength frequency-domain THz imaging for the detection and identification of materials in a reflection geometry.

Acknowledgements

We acknowledge support from the Research Councils (UK) Basic Technology Programme, the Engineering and Physical Sciences Research Council (EPSRC, UK), and Her Majesty's Government Communication Centre (HMGCC, UK).

#92353 - $15.00 USD Received 1 Feb 2008; revised 5 Mar 2008; accepted 5 Mar 2008; published 14 Apr 2008